IEEE Access
Multidisciplinary | Rapid Review | Open Access Journal

Received May 3, 2020, accepted May 23, 2020, date of publication May 29, 2020, date of current version June 15, 2020.

Digital Object Identifier 10.1109/ACCESS.2020.2998510

Differential Drive Based Yaw Stabilization Using MPC for Distributed-Drive Articulated Heavy Vehicle

TAO XU, (Member, IEEE), XUEWU JI, YULONG LIU, AND YAHUI LIU, (Member, IEEE)
State Key Laboratory of Automotive Safety and Energy, Tsinghua University, Beijing 100084, China

Corresponding author: Yahui Liu (liuyahui@tsinghua.edu.cn)

This work was supported in part by the National Key Research and Development Program of China under Grant 2017YFB0103900, and in part by the National Natural Science Foundation of China under Grant 51875302.

ABSTRACT This paper presents a differential drive approach for distributed-drive articulated heavy vehicles (DAHVs) with wheel-side motors. The objective is to keep the yaw stability for DAHVs with direct yaw moment in driving process when the external disturbance acts on one of the vehicle parts. Three contributions are made in this paper: 1) An disturbance observer based Extended Kalman Filter (EKF) strategy is implemented to deal with the unknown mismatched disturbances in strong nonlinear vehicle system for DAHVs; 2) The differential drive approach is developed with the guidance of model predictive controller (MPC) to cope with the vehicle instability with the decoupling dynamic analyses for DAHVs under the observed external disturbance and the specific drive limitation of wheel-side motor for the first time; 3) The novel verification techniques with co-simulation model combining with the ADAMS, Simulink, and AMESim software for DAHVs is employed to verify this vehicle stability controller, which is more reasonable than the traditional methods with simple virtual model. The results demonstrate that the proposed approaches can reduce the oscillation amplitude and period of vehicle yaw motion for about 40% and 80%, respectively. Moreover, the MPC strategy is more efficient comparing with the LQR strategy especially on boundaries issue treatment, which can improve the vehicle stability greatly.

INDEX TERMS Distributed-drive articulated heavy vehicle, model predictive controller, differential drive, yaw stabilization.

I. INTRODUCTION

With the gradually changing of "Intelligent Mine" from concept to reality, the innovative development of engineering machinery arouse more and more attention [1], [2]. As the new mechanical equipment in mining industry, the distributed-drive articulated heavy vehicles (DAHVs) and its good vehicle performance become particularly important. However, due to the special structure of two vehicle parts connected by two hydraulic struts and one articulation joint without locking mechanism [3]–[5], the front and rear vehicle parts can rotate relatively, which easily make DAHVs produce oscillatory yaw motion during moving process, especially with the external disturbance. Moreover, the hydraulic struts is inevitably entrained with gas and produce leaks, which can decrease the vehicle torsional stiffness and increase the oscillatory yaw motion or even lead to instability for DAHVs [6], [7].

The special vehicle structure including hydraulic steering system of DAHVs is indispensable in improving vehicle performance of manoeuvrability, although there are some problems in vehicle yaw stability [6]. Therefore, it is important to take some strategies to improve the vehicle performance with the existing condition, which can be grouped into two categories in now researches, including active and passive prevention methods. Some literatures make compensation of hydraulic oil for two struts to keep the torsional stiffness of DAHVs, which can reduce the influence of the leaks and entrained gas in hydraulic oil [8], [9]. Moreover, some literatures even increase the friction of articulation joint directly to make DAHVs more like traditional rigid cars and reduce the influence of small external disturbance on vehicle stability [7], [10]. These methods change the vehicle parameters actively and improve the vehicle performance but

The associate editor coordinating the review of this manuscript and approving it for publication was Francesco Tedesco.

produce energy waste and cannot be used widely. For the unavoidable oscillatory yaw motion of DAHVs, some positive methods, including active steering [11], and differential braking [12]–[15] can be taken to keep the vehicle stability. These methods use the direct yaw moment produced by the differential braking or driving methods to overcome the oscillatory yaw motion, which can be widely used in traditional articulated heavy vehicles. But for the DAHVs, the most significant feature is that each wheel of the vehicle can be controlled by the wheel-side motor independently [16]. And the direct yaw moment can be easily produced in front and rear vehicle parts. Consequently, it is possible for DAHVs to realize the more accurate control in keeping vehicle stability.

Therefore, this paper takes full advantages of independent drive characteristics of DAHVs to establish a yaw stability controller with the application of MPC strategy. Firstly, the nonlinear vehicle dynamic mathematic model and a novel verification technique with co-simulation virtual model are developed combining with the previous studies. These models are also verified by field test. Secondly, the co-simulation virtual model is implemented to analyze the yaw stability by comparing the articulation angle of DAHVs with different vehicle parameters. In order to simulate the oscillatory yaw motion in the predictive model of the controller, EKF method is used to observe the external disturbance for the strong nonlinear vehicle system. With the linearization and discretization of the vehicle mathematic model, the differential drive controller based on MPC strategy is designed. Case study with special vehicle parameters and certain external disturbance is implemented to verify the controller in the end.

The rest of this paper is organized as follows. The vehicle dynamic mathematic model, co-simulation virtual model, and field test for the models are described in Section II. In Section III, the influence of different parameters on the vehicle stability is analyzed by the co-simulation virtual model. The differential drive approach with EFK and MPC is proposed in Section IV. In Section V, simulations with co-simulation model platform are conducted. Followed is the conclusion in Section VI.

II. THE MODEL OF DAHVs

A. MATHEMATICAL MODEL OF DAHVs

This section presents a mathematical model of vehicle dynamics and hydraulic steering system for DAHVs. The vehicle is driven by all wheels with independent wheel-side motors. Its steering motion is realized with the coupling effect of hydraulic struts and articulation joint, which have been introduced in literature [3], [17]. In terms of the traditional design of AHVs, there is no suspension in the chassis system. The vertical, roll and pitch motions of vehicle and their effects on steering systems can be neglected. A 6-DOF (degree of freedom) mathematical model with consideration of the yaw, longitudinal and lateral vehicle dynamics is adopted for the control design as shown in Fig. 1. Its mathematical model can be described using the following (1).

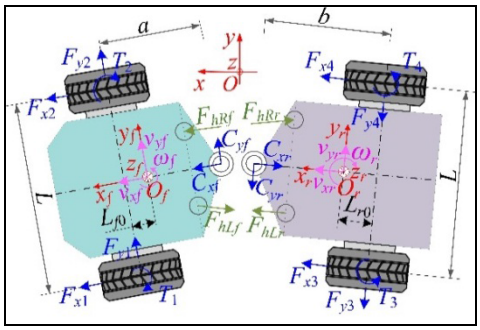

FIGURE 1. Schematic of DAHVs dynamic model.

$$\begin{cases} m_f\left(\dot{v}_{xf}+v_{yf}\omega_f\right)=C_{xf}+F_{hxf}+F_{wxf} \\ m_f\left(\dot{v}_{yf}-v_{xf}\omega_f\right)=C_{yf}+F_{hyf}+F_{wyf} \\ I_{zf}\dot{\omega}_f=-\left(T_1+T_2\right)+T_{Cyzf}+T_{hzf}+T_{wyzf}+T_{wxzf} \\ m_r\left(\dot{v}_{xr}-v_{yr}\omega_r\right)=-C_{xr}+F_{hxr}+F_{wxr} \\ m_r\left(\dot{v}_{yr}+\omega_r v_{xr}\right)=-C_{yr}+F_{hyr}+F_{wyr} \\ -I_{zr}\dot{\omega}_r=T_3+T_4+T_{Cyzr}+T_{hzr}+T_{wyzr}+T_{wxzr} \end{cases} \tag{1}$$

where m_f and m_r represent the vehicle mass, while f and r represent the front and rear parts of the vehicle, respectively, which is same as the following analyses. v_{xf}, v_{yf} and ω_f are the longitudinal velocity, lateral velocity, and yaw rate of front part of the vehicle, which are same as the meaning of v_{xr}, v_{yr} and ω_r for the rear part. Because of the special structure of vehicle model, the longitudinal and lateral velocity (v_{xr}, v_{yr}) of rear part can be derived by (2). C_{xf}, C_{yf}, C_{xr} and C_{yr} stand for the forces at articulation joint in front and rear parts of the vehicle, respectively. F_{hx} and F_{hy} denote the forces of hydraulic struts along the x-axis and y-axis of the coordinate system, respectively. F_{wx} and F_{wy} represent the wheel forces along the same direction as F_{hx} and F_{hy}, respectively. I_z is the mass moment of inertia. T_{wyz}, T_{wxz}, T_{hz}, and T_{Cyz} are the moments around the z_f-axis coordinate system, which are produced by the wheels, hydraulic struts, and articulation joint, respectively.

$$\begin{cases} v_{xr}=v_{xf}\cos\left(\theta\right)+\left(v_{yf}+\omega_f\cdot\left(a-L_{f0}\right)\right)\sin\left(\theta\right) \\ v_{yr}=-v_{xf}\sin\left(\theta\right)+\left(v_{yf}+\omega_f\cdot\left(a-L_{f0}\right)\right)\cos\left(\theta\right) \\ -\ldots-\omega_r\left(a-L_{f0}\right) \end{cases} \tag{2}$$

where θ represents the articulation angle of the vehicle. Based on the analyses above, the vehicle dynamics of (1) can be modeled as

$$R\dot{X}=G'\left(X\right)+GP+H \tag{3}$$

where $X=[v_{xf},\ v_{yf},\ \omega_f,\ \omega_r]^{\mathrm{T}}$ represents the vehicle state, while $G'\left(X\right)$ denotes the vector about X that can be expressed by (5). $P=[P_{in},\ P_{out}]^T$ represents the pressure in piston-side chamber of right strut or rod-side chamber of left strut, while P_{out} is the pressure in piston-side chamber of left strut or rod-side chamber of right strut of hydraulic struts. R,

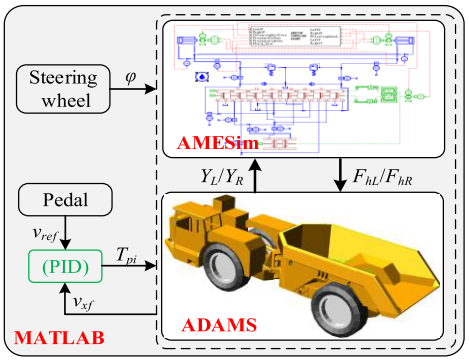

FIGURE 2. The diagram of the co-simulation model.

H, and G are the constant matrix, which can be expressed by Appendix (I-1), (I-2) and (4).

$$G = \begin{bmatrix} a_{11} & a_{12} & a_{13} & a_{14} & a_{15} & a_{16} \\ a_{21} & a_{22} & a_{23} & a_{24} & a_{25} & a_{26} \end{bmatrix}^T \quad (4)$$

$$G'(X) = \begin{bmatrix} a_{31} & a_{32} & a_{33} & a_{34} & a_{35} & a_{36} \end{bmatrix}^T \quad (5)$$

where a_{11}- a_{26} are the constant, while $a_{31} - a_{36}$ denote the state function, which can be expressed by appendix (I-3).

B. CO-SIMULATION MODEL OF DAHVs

In current research works, there are no common simulation software, i.e., Carsim or Trucksim, which can be used to make verification for the study of DAHVs. Meanwhile, the limitation of experimental makes it necessary to study a new verification technique for DAHVs [18], [19]. ADAMS is the simulation software that concentrates on the mechanical dynamics analyses while AMESim contribute to the research of hydraulic system, which can be used to build a co-simulation model for the verification of the studies of DAHVs. In this co-simulation model, the vehicle model, tire model, and road are built in ADAMS while AMESim is used to build the model of steering unit, hydraulic structs, and accumulator. Moreover, MATLAB is implemented to control the vehicle body and translate the information between these two simulation models. Its diagram is shown in Fig. 2. In this virtual prototype, φ is steering wheel angle, which is used to control the steering unit of hydraulic steering system in AMESim. v_{ref} and v_{xf} are the reference velocity and the real velocity from ADAMS, respectively. These two parameters determine the driving torque of each wheel T_{pi} with the PID controller. F_{hL} and F_{hR} are the forces of hydraulic struts calculated by AMESim, which provide the steering driving forces for the vehicle model in ADAMS. And the corresponding struts length Y_L and Y_R are obtained from ADAMS and output back to AMESim to achieve the movements of hydraulic struts in next step.

C. FIELD TEST

In order to verify the mathematical model and co-simulation model, field tests are performed with a loaded 35t DAHVs.

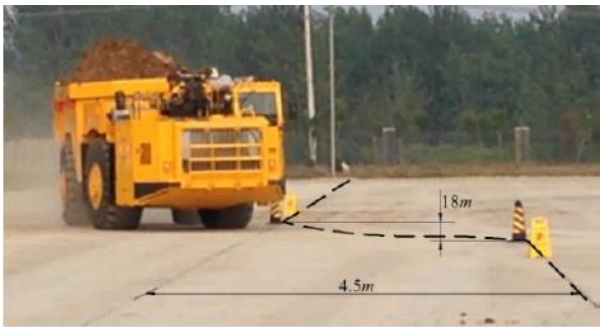

FIGURE 3. Experimental area of field test.

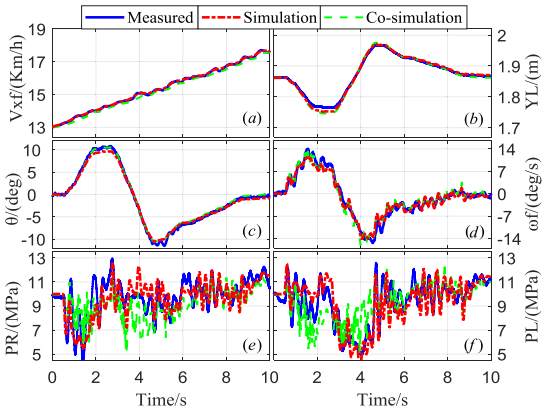

FIGURE 4. Response comparison of simulations and measured data. (a) the vehicle velocity, (b) the length of hydraulic strut, (c) the articulation angle (d) yaw rate of the vehicle front part, (d) the pressure of right strut, (e) the pressure of right strut.

The experimental area is shown in Fig. 3. The parameters of vehicle and hydraulic steering system can refer to the literature [3]. With these parameters, the mathematical model in MATLAB/Simulink and virtual co-simulation model are established. The comparisons of the simulation results with measure data are shown in Fig. 4.

This field test was conducted on a cement road with a fully loaded articulated vehicle. The vehicle was turned to the left for about 1.5 s and kept in the steady steering state for about 0.5 s. Then, the steering wheel was turned back to the right side. The vehicle speed was under 18 km/h in this filed test. The input of steering wheel angle and the vehicle velocity in this field test are shown in Fig. 9 in literature [3]. The comparison among the experimental data, simulations of the mathematical model and co-simulation model are illustrated in Fig. 4.

Fig 4(a) is the comparison of vehicle velocity from the virtual model and experimental data during steering process. The maximum error is under 2%. Fig. 4(b) shows the changes in length of left-strut based on the inputs of the field test. It decreases and then increases during steering process. And the maximum errors between the mathematical model, co-simulation model, and measurement data are about 8 mm and 10 mm, respectively, which accounting for 0.45% and 0.5%

of its length at 2.7 s. Fig. 4(*c*) shows the changes in the articulation angle of the vehicle. The maximum errors among the mathematical model, co-simulation model and experimental data are approximately 4% and 5%, respectively. Fig. 4(*d*) compares the simulations results and experimental data of yaw rate for the front part of the vehicle. Its value is the differential of the steering angle of the vehicle front part. Because of the possible measuring errors, there exist some disagreement between the simulations and experimental data. The maximum errors are about 8% and 6%, respectively. Fig. 4(*e*) and (*f*) shows the pressure of the left strut. The initial pressure of the hydraulic steering system is 10MPa, which is the same as the parameters of the field test vehicle in literatures [3].

According to the agreements of these simulation results and measured data in Fig. 4, the negligible error could validate that the mathematic and virtual co-simulation models described above are accurate compared to the real steering process of DAHVs. These models can be used to verify the studies for DAHVs, which are introduced in the following sections.

III. STABILITY ANALYSES FOR DAHVs

Compared with the traditional cars, DAHVs are equipped with two hydraulic struts and one articulated joint, which permit the front and rear vehicle parts to rotate relatively. This characteristic makes it good performance of manoeuvrability but decrease the vehicle torsional stiffness. For smaller disturbance, the resulting disturbed motion may be a snaking mode [12], [20] or even lead to instability during steady state straight moving. Some literatures have studied this vehicle behaviour with the influence of disturbance under different vehicle parameter. For instance, Gao *et al.* [9] studied the bulk modulus of hydraulic steering system under different air content of oil and analysed its influences on the vehicle snaking mode with the consideration of vehicle velocity. Azad *et al.* [10] analysed the effects of centre of the mass, and the moment of inertia on the snaking mode of DAHVs. Crolla and Horton [20] made the researches on the effective vehicle torsional stiffness and its influence on the snaking instabilities. And they pointed out that the entrapped air and flexible pipes in hydraulic system were the main factors that result in low stiffness for the DAHVs. In short, the special structural features of DAHVs make it more flexible but easily lead to stability problems. Therefore, combining with the analyses in previous studies and the co-simulation model in this manuscript, summary the characteristics of vehicle snaking mode with small disturbance under different parameters for DAHVs, which are shown in Fig. 5.

Fig. 5 (*a*) shows the vehicle moving behaviour under fully loaded or unloaded conditions. It shows that with the increase of load, the influence of disturbance on vehicle moving process is decreased but the oscillation of the vehicle yaw motion is strengthen, which is more like a snaking mode. Fig. 5(*b*) is the vehicle moving behaviour with the influence of different air content in oil of hydraulic steering system. With the

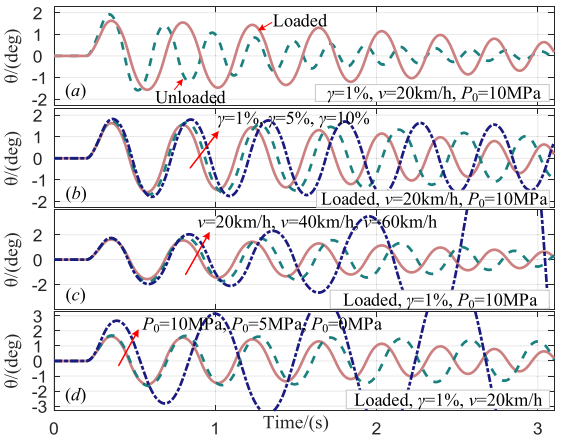

FIGURE 5. Snaking mode of DAHVs under different conditions.

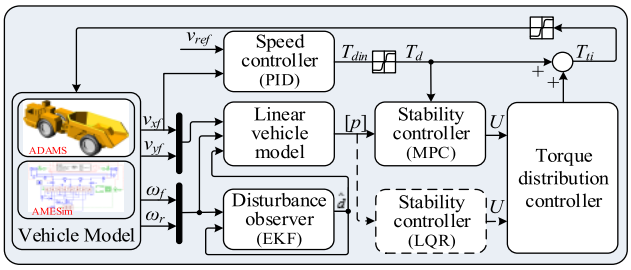

FIGURE 6. Block diagram of the complete controller for DAHVs.

comparison of oil, the air is easily compressed, which lead to the low torsional stiffness of vehicle body for DAHVs and make the vehicle instability during moving process. Moreover, based on the previous studies introduced above, it can be known that the vehicle velocity is the critical factor that influences the vehicle stability, which is same as the simulation in this manuscript shown in Fig. 5(*c*). The vehicle response is the obvious snaking mode when the velocity is 20km/h. However, the amplitude of the motion oscillation will grow with the increase of vehicle velocity, and when it reaches to 60km/h or higher, the vehicle will show instability. But the maximum velocity of DAHVs is limited at 35km/h. So the vehicle always shows the snake mode with small disturbance. Fig. 5(*d*) presents the influence of hydraulic pressure in struts on the vehicle moving process. The lower pressure in struts can lead to the lower vehicle torsional stiffness, which is same as the influence of air content in oil.

Whatever the reasons that lead to the vehicle instability, it all due to the yaw moment produced by external disturbance that generate the additional yaw motion. Therefore, the active yaw moment controlled by differential driving forces of wheels can be used to overcome its improper moving process, which is the main content of next sections.

IV. YAW STABILITY CONTROL FOR DAHVs

This section presents the yaw stability control methods and its verification technology for DAHVs. The block diagram

to illustrate the procedure of this complete control strategy is shown in Fig. 6. In this figure, the co-simulation model introduced above is object that replaces the real test vehicle for the verification of the controller. In the control system, PID method is implemented to keep the target velocity of the vehicle. Meanwhile, the mathematic model introduced above is used to design the stability controller based on the MPC method. It is mainly used for the calculation of appropriate active yaw moment for the yaw stability of DAHVs, which is contrasted by the stability controller with LQR method. The EKF method is used to estimate the real external disturbance for the real-time control of the vehicle, which is the demand parameter of MPC controller. The specific research contents are shown as following.

A. THE SUPERVISORY CONTROLLER BASED ON PID

The supervisory controller is used to control the vehicle velocity with the comparison of the velocity of vehicle front part and the referent vehicle velocity. The output of this controller is demand drive torque T_{din} of each wheel it is always limited by the drive ability of wheel-side motor whether the stability controller exist or not. The real drive torque used to keep the vehicle velocity is T_d, which is the constraint of MPC controller.

B. THE UPPER CONTROLLER DESIGN

The upper controller is designed for the calculation of the direct yaw moment. It includes two parts: the disturbance observer based on EKF and the stability controller based on MPC.

1) DISTURBANCE OBSERVER DESIGN BASED ON EKF

EKF, the common estimation technology, is implemented to estimate the equivalent additional yaw moment of different vehicle parts produced by external disturbance during moving process. EKF is an efficient recursive algorithm and appropriate for the nonlinear vehicle system [21]–[23], which is suitable for the design of disturbance observer for DAHVs.

When the external disturbance act on the vehicle, the vehicle dynamic model (equation(3)) can be rewritten by

$$R\dot{X} = G'(X) + GP + H + M \tag{6}$$

where $M = [0, 0, \Delta Mf, 0, 0, \Delta Mr]^T$ represents the equivalent external disturbance torque, and ΔM_f is for the front vehicle part while ΔM_r is for the vehicle rear part.

By solving (6), the vehicle dynamic model with external disturbance can be rewritten by

$$\dot{X} = f(X) = \left(KD + K'\right)\left(G'(X) + GP + M\right) \tag{13}$$

where K, D, and K' are shown in Appendix (I-4), (I-8) and (I-9), respectively.

Assume that the external disturbance acted on the vehicle is constant at each step time. And the state variables can be presented by (14) with the consideration of requirement of EKF.

$$X_{ekf} = \begin{bmatrix} v_{xf} & v_{yf} & \omega_f & \omega_r & M_f & M_r \end{bmatrix} \tag{14}$$

The vehicle dynamic model can be changed by

$$\dot{X}_{ekf} = \begin{bmatrix} \dot{X} \\ \dot{M}_f \\ \dot{M}_r \end{bmatrix} = \begin{bmatrix} f\left(X, M_f, M_r\right) \\ 0 \\ 0 \end{bmatrix} = f_{ekf}\left(X_{ekf}\right) \tag{15}$$

Taking the capabilities of sensors into consideration, the yaw rate of front and rear vehicle parts is chosen as the measurement variables and define the measurement matrix $z = [\omega_f, \omega_r]^T$. With the discretization of vehicle dynamic model of (15), the vehicle state-space equation for the calculation of EFK can be expressed by

$$\begin{cases} \dot{X}_{ekf(k)} = f\left(X_{efk(k-1)}\right) + w_{ekf(k-1)} \\ z_{(k)} = H_{ekf} X_{(k-1)} + v_{ekf(k-1)} \end{cases} \tag{16}$$

where w_{ekf} and v_{ekf} are the white noise of the system. The means of these two sets of white noise are 0 and the covariance are Q_{ekf} and R_{ekf}, respectively. H_{ekf} is the coefficient matrix, which can be expressed by (17).

$$H_{ekf} = \begin{bmatrix} 0 & 0 & 1 & 0 & 0 & 0 \\ 0 & 0 & 0 & 1 & 0 & 0 \end{bmatrix} \tag{17}$$

With the reference of literature [23], the step of EKF algorithm is presented in Table 1.

TABLE 1. The step of EKF algorithm.

Step 1: Prediction of the state variables

$$X^-_{ekf(k)} = f_{ekf}\left(X_{(k-1)}\right) \tag{7}$$

Step 2: Prediction of the error covariance (P_{ekf})

$$P^-_{ekf(k)} = \Phi_{ekf(k)} P_{ekf(k-1)} \Phi^T_{ekf(k)} + Q_{ekf} \tag{8}$$

where $\Phi_{ekf}=I+T_sF$. I is the identity matrix. T_s is the simulation step size. F is the Jacobian of function f_{ekf}, which can be defined by (9). Its value is shown in Appendix (I-7)

$$\Phi_{ekf} = \partial f_{ekf} / \partial X_{ekf} \tag{9}$$

Step 3: Calculation of Kalman gain (K_{ekf})

$$K_{ekf(k)} = P^-_{ekf(k)} H^T_{ekf}\left(H_{ekf} P^-_{ekf(k)} H^T_{ekf} + R_{ekf(k)}\right)^{-1} \tag{10}$$

Step4: Update the state variables

$$X_{ekf(k)} = X^-_{ekf(k)} + K_{ekf(k)}\left(z_{(k)} - H_{ekf} X^-_{ekf(k)}\right) \tag{11}$$

Step5: Update the covariance matrix

$$P_{ekf(k)} = \left(I - K_{ekf(k)}\right) P^-_{ekf(k)} \tag{12}$$

2) STABILITY CONTROLLER DESIGN BASED ON MPC

This section studies the yaw stability controller for DAHVs by differential control of right- and left- side of wheels. This controller is used to calculate the appropriate direct

yaw moment based on MPC for the front and rear vehicle parts to decrease the influence of external disturbance and keep the vehicle stability. With the effect of this direct yaw moment, the vehicle dynamic model can be rewritten by (18) combining with the (3) and (6).

$$R\dot{X} = G'(X) + GP + H + EU \tag{18}$$

where $U = [\Delta Mf + Mf,\ \Delta Mr + Mr]^T$, and the M_f and M_r represent the direct yaw moment for the front and rear vehicle parts, respectively. E is constant matrix, which can be expressed by:

$$E = \begin{bmatrix} 0 & 0 & 0 & 0 & 0 & 1 \\ 0 & 0 & 1 & 0 & 0 & 0 \end{bmatrix}^T \tag{19}$$

Equation (18) shows the coupling effect between the force of hydraulic struts and direct yaw moment on the vehicle moving process. With the decoupling analysis, it can be rewritten by:

$$\dot{X} = \left(KD + K'\right)\left(G'(X) + GP + EU\right) \tag{20}$$

a: MODEL OF THE WHOLE SYSTEM

In the normal moving process, the longitudinal velocity of DAHVs can be kept constant by the driver, which has been introduced above. The yaw stability of the vehicle is related with its lateral velocity and yaw rate of the vehicle. Define $y_1 = v_{yf}$, $y_2 = \omega_f$, and $Y = [v_{yf}, \omega_f]$, the system dynamics model of DAHVs can be expressed by (21) combining with the decoupling analyses above.

$$\begin{cases} \dot{X} = \left(KD + K'\right)\left(G'(X) + GP + EU\right) \\ Y = CX \end{cases} \tag{21}$$

where

$$C = \begin{bmatrix} 0 & 1 & 0 & 0 \\ 0 & 0 & 1 & 0 \end{bmatrix} \tag{22}$$

Considering the requirements of real-time simulation of this system, the linear model predictive control (LMPC) method is used to design this controller. Correspondingly, the nonlinear vehicle system dynamic model of (14) needs to be linearized to satisfy the requirements of LMPC. Taylor's formula is carried out on this nonlinear system dynamic model, which is expanded at initial point of state (X_0, U_0). When the higher order terms are ignored, the first order and constant of this system can represent the linear system dynamic vehicle model, which can be expressed by,

$$\begin{cases} \dot{x} = A_{mpc}x + B_{mpc}u + D_{mpc} \\ y = C_{mpc}x \end{cases} \tag{23}$$

where $x = X\text{-}X_0$, $u = U\text{-}U_0$, and $y = Y$ are state variables, input and output matrix, respectively. The A_{mpc}, B_{mpc}, and D_{mpc} are the state parameters related with the original dynamic model, which can be expressed by (24)∼(26). With the solve of (24) and (25), the matrix A and B can be derived by Appendix (I-10) and (I-11).

$$A_{mpc} = \left(KD + K'\right)\left[\frac{\partial\left[G'(X)\right]}{\partial X}\Big|_{X=[v_{xf},v_{yf},\omega_f,\omega_r]}\Bigg|_{\substack{X=X_0\\U=U_0}}\right] \tag{24}$$

$$B_{mpc} = \left(KD + K'\right)E\left[\frac{\partial(U)}{\partial U}\Big|_{U=[\Delta M_f,\Delta M_r]}\Bigg|_{\substack{X=X_0\\U=U_0}}\right] \tag{25}$$

$$D_{mpc} = \left(KD + K'\right)\left(G'(X_0) + GP + EU_0\right) - A_{mpc}X_0 \tag{26}$$

Considering the calculation requirements of MPC, the vehicle system dynamic model (equation (23)) needs to be discretised in a certain sampling period T_s with the guidance of (27).

$$\dot{x}(kT_s) = \lim_{T_s\to 0}\frac{[x[(k+1)T_s] - x(kT_s)]}{T_s}\Bigg|_{k=0,1,2\cdots} \tag{27}$$

Combining with the (27), the time-varying system of (23) can be discretised by:

$$\begin{cases} x[(k+1)T_s] = \underbrace{\left(I + A_{mpc}T_s\right)}_{A_{kt}}x(kT_s) \\ \qquad + \underbrace{B_{mpc}T_s}_{B_{kt}}u(kT_s) + \underbrace{D_{mpc}T_s}_{D_{kt}} \\ y[(k+1)T_s] = C_{kt}x[(k+1)T_s] \end{cases} \tag{28}$$

where $I = \mathrm{diag}\{1,1,1,1\}$, $C_{kt} = C$.

b: THE OBJECTIVE FUNCTION AND CONSTRAINT

The stability controller of DAHVs is used to reduce the influence of external disturbance and make the lateral velocity and yaw rate to be zero. The objective function of this MPC controller for DAHVs is defined below:

$$J(k) = [y(k)]^T\tilde{Q}[y(k)] + \cdots + [u(k)]^T \times\tilde{R}[u(k)] + [\Delta u(k)]^T\tilde{S}[\Delta u(k)] \tag{29}$$

s.t.

$$lb \le u(k) \le ub \tag{30}$$

$$lb = \begin{bmatrix} M_{f\min} & M_{r\min} \end{bmatrix}^T \tag{31}$$

$$ub = \begin{bmatrix} M_{f\max} & M_{r\max} \end{bmatrix}^T \tag{32}$$

where the terms on the right side in (29) are the output cost, input cost, and cost of the increment of input, respectively. $\tilde{Q}$, $\tilde{R}$ *and* $\tilde{S}$ *are* weights to balance each term. *lb* and *ub* in (30) are the boundaries of input, which are related with the direct yaw moment in front and rear vehicle parts expressed by (32).

TABLE 2. The gains of EKF and MPC algorithms.

T_s	0.005
Q_{ekf}	diag{10^{-5}, 10^{-5}, 10^{-5}, 10^{-5}, 10^{12}, 10^{12}}
R_{ekf}	diag{7×10^{-5}, 7×10^{-5}}
$\tilde{Q}$	diag{3×10^5, 3×10^5}
$\tilde{R}$	diag{1, 1, 1, 1}×10^{-7}
$\tilde{S}$	diag{0, 0, 1, 1}

C. THE LOWER CONTROLLER OF THE TORQUE DISTRIBUTION DESIGN

The lower controller of this paper is designed for the direct yaw moment distribution obtained from the stability controller. In order to reduce its influence on the longitudinal dynamics of DAHVs, the strategy of torque distribution can be expressed by (33) combining with the outputs of PID controller T_d.

$$\begin{cases} T_{t1} = T_d - \Delta M_f/L \\ T_{t2} = T_d + \Delta M_f/L \\ T_{t3} = T_d + \Delta M_r/L \\ T_{t4} = T_d - \Delta M_r/L \end{cases} \tag{33}$$

where T_{t1}, T_{t2}, T_{t3}, and T_{t4} are required torque of front-left, front-right, rear-left, and rear-right wheels, respectively. L is the wheel track of DAHVs.

V. CASE STUDY

In this section, the co-simulation model is implemented to verify the effectiveness of the stability controller. In the simulation, the vehicle moves on the straight line when the perturbation acted on one side of front or rear vehicle part. Once this situation occurs, the controller will work to produce the direct yaw moment to keep the vehicle stability. The control objective is to reduce the vehicle oscillation during moving process. The vehicle structure parameters used in the co-simulation can refer to the literature [3]. Due to the physical limitation of wheel-side motor, the output saturation issue is considered in the controller, and the maximal value of the direct yaw moment for the front and rear vehicle parts are all chosen as 146.7kNm (the maximum output torque of wheel-side motor is 2577Nm, the tyre effective radius is 1.032m, and the gear ratio is 25, which has been introduced in literature [17]). For the upper controller, including EKF and MPC algorithms, the gains are chosen according to the structure characteristics of DAHVs, which are shown in Table 2.

In order to highlight the superiority of the MPC controller, the LQR approach is used to conduct a comparative simulation. The reason for choosing LQR is that it can yield good performance in vehicle stability control for DAHVs, which has been introduced in literature [6]. And the advantage of the MPC approach compared with LQR is not very large [6], [24]. But there are also two reasons for using MPC algorithm instead of LQR to achieve the control objective in this paper.

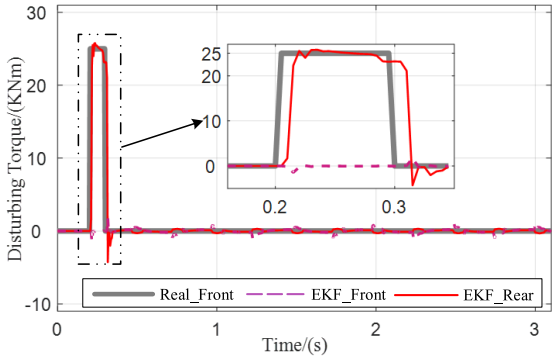

FIGURE 7. Results of the external disturbing torque observed by EKF in the simulation.

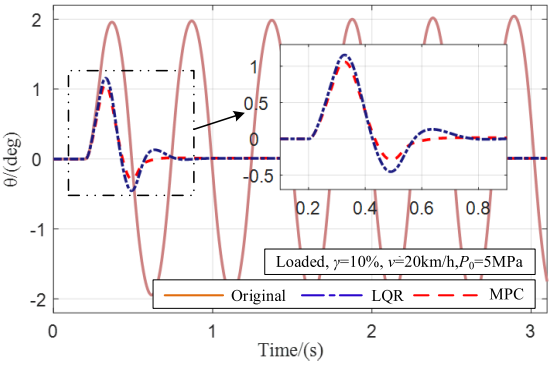

FIGURE 8. Results of the articulation angle under different controller in the simulation.

1) the MPC approach can make the actual vehicle state closer to the reference than LQR approach because of its rolling optimization technology in a simulation step; 2) the MPC approach can deal with the output saturations of drive wheels with wheel-side motor, while LQR approach might easily exceed the actuator limit of its drive ability.

With the introduction above, we make simulation with the loaded vehicle run on the cement road (the tire-road friction coefficient $\mu = 0.7$) and straight line. Its front vehicle part is subjected an external disturbing torque (25kNm) at 0.2s. After that, the controller is activated and makes the vehicle stability. Because of the maximum vehicle velocity of DAHVs is imitated at 35km/h. So the normal vehicle velocity in this simulation is chosen as 20km/h. Otherwise the air content of hydraulic oil is chosen as 10%, and the pressure in struts is chosen as 5Mpa.

The comparing results of the external disturbing torque for the front and rear vehicle parts between the real parameter and the observed value by EKF are shown in Fig. 7. From the results, it is found that this EKF observer is effective to make the observed value track the real parameter even there is one or two step (0.005∼0.01s) delay, which can provide appropriate reference for the stability control of DAHVs.

The results of the articulation angle with or without yaw stability controller are shown in Fig. 8. From the simulation

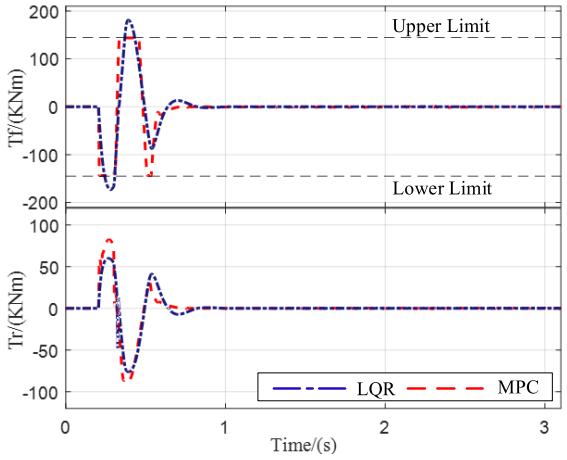

FIGURE 9. Results of control inputs of front and rear vehicle parts provided by wheel-side motor in the simulation.

results, one can observed that, the vehicle moving process shows the oscillation with the increased amplitude of articulation angle under the parameters above without stability controller. And the vehicle will be instability in next step. But when the yaw stability controller is implemented into the vehicle, its articulation angle can recover the original steady-state moving process after one period of oscillation. And its oscillation amplitude and period can be reduced for about 40% and 80%, respectively. From the simulation results, it also can be observed that LQR strategy can already keep the vehicle stability, however, the MPC approach can further reduce the vehicle oscillation amplitude and period, which is related to the control of boundaries issue treatment of actuator limitation. As for the control inputs of different vehicle parts provided by wheel-side motor, it is validated that the MPC strategy can maintain this control inputs with the actuator limitation, shown as Fig. 9, which is hard for the LQR strategy.

VI. CONCLUSION

The goal of this study is to present a yaw stability controller for DAHVs with the application of MPC strategy, which was realised with the direct yaw moment produced by differential driving forces of independently wheel-side motor.

$$R = \begin{bmatrix} m_1 & 0 & 0 & 0 \\ 0 & m_1 & 0 & 0 \\ 0 & 0 & I_{zf} & 0 \\ m_2\cos(\theta) & m_2\sin(\theta) & m_2\left(a - L_{f0}\right)\sin(\theta) & -\cos(\theta) \\ -m_2\sin(\theta) & m_2\cos(\theta) & m_2 L_f\cos(\theta) & -m_2 L_r \\ 0 & 0 & 0 & -I_{zr} \end{bmatrix} \tag{I-1}$$

$$H = \begin{bmatrix} C_{xf} \\ C_{yf} \\ \left(a - L_{f0}\right) C_{yf} \\ -\cos(\theta)\, C_{xf} - \sin(\theta)\, C_{yf} \\ \sin(\theta)\, C_{xf} - \cos(\theta)\, C_{yf} \\ -\left(b - L_{rO}\right)\sin(\theta)\, C_{xf} + \left(b - L_{rO}\right)\cos(\theta)\, C_{yf} \end{bmatrix} \tag{I-2}$$

$$\begin{cases} a_{11} = -A_p\cos\left(\theta_{fL}\right) + A_a\cos\left(\theta_{fR}\right), \quad a_{21} = A_a\cos\left(\theta_{fL}\right) - A_p\cos\left(\theta_{fR}\right), \; a_{31} = F_{wxf} - m_1 v_{yf}\omega_f, \\ a_{12} = A_p\sin\left(\theta_{fL}\right) - A_a\sin\left(\theta_{fR}\right), \quad a_{22} = -A_a\sin\left(\theta_{fL}\right) + A_p\sin\left(\theta_{fR}\right), \; a_{32} = F_{wyf} + m_1 v_{xf}\cdot\omega_f \\ a_{13} = A_p\cdot\cos\left(\theta_{fL}\right)\cdot L_{fL} + A_a\cdot\cos\left(\theta_{fR}\right)\cdot L_{fR} + \left(A_p\sin\left(\theta_{fL}\right) - A_a\sin\left(\theta_{fR}\right)\right)\left(a - L_{fO} - a_f\right), \\ a_{23} = -A_a\cos\left(\theta_{fL}\right)\cdot L_{fL} - A_p\cos\left(\theta_{fR}\right)\cdot L_{fR} + \left(-A_a\sin\left(\theta_{fL}\right) + A_p\sin\left(\theta_{fR}\right)\right)\left(a - L_{fO} - a_f\right), \\ a_{33} = (T_1 + T_2) + T_{wyzf} + T_{wxzf}, a_{14} = A_p\cos\left(\theta_{rL}\right) - A_a\cos\left(\theta_{rR}\right), \\ a_{24} = -A_a\cos\left(\theta_{rL}\right) + A_p\cos\left(\theta_{rR}\right), \\ a_{34} = F_{wxr} + m_2 v_{yr}\omega_r + m_2\left(\omega_f + \omega_r\right)\left(v_{xf}\sin(\theta) - \left(v_{yf} + \omega_f\cdot L_f\right)\cos(\theta)\right), \\ a_{15} = -A_p\sin\left(\theta_{rL}\right) + A_a\sin\left(\theta_{rR}\right), \quad a_{25} = A_a\sin\left(\theta_{rL}\right) - A_p\sin\left(\theta_{rR}\right), \\ a_{35} = F_{wyr} - m_2 v_{xr}\omega_r + m_2\left(\omega_f + \omega_r\right)\left(v_{xf}\cos(\theta) + \left(v_{yf} + \omega_f\cdot L_f\right)\sin(\theta)\right), \\ a_{16} = -A_p\cos\left(\theta_{rL}\right)\cdot L_{rL} - A_a\cos\left(\theta_{rR}\right)\cdot L_{rR} + \left(A_p\sin\left(\theta_{rL}\right) - A_a\sin\left(\theta_{rR}\right)\right)\left(b - L_{rO} - b_r\right), \\ a_{26} = A_a\cos\left(\theta_{rL}\right)\cdot L_{rL} + A_p\cos\left(\theta_{rR}\right)\cdot L_{rR} + \left(-A_a\sin\left(\theta_{rL}\right) + A_p\sin\left(\theta_{rR}\right)\right)\left(b - L_{rO} - b_r\right), \\ a_{36} = (T_3 + T_4) + T_{wyzr} + T_{wxzr} \end{cases} \tag{I-3}$$

$$K = \begin{bmatrix} K_{11} & K_{12} & K_{13} \\ K_{21} & K_{22} & K_{23} \\ K_{31} & K_{32} & K_{33} \\ K_{41} & K_{42} & K_{43} \end{bmatrix} \tag{I-4}$$

This paper is the first one to bring the intelligent control methods, including EKF and MPC, into DAHVs for its yaw stability. In this paper, the vehicle dynamic mathematic model and co-simulation virtual model are firstly discussed briefly and verified by field test. As the verification techniques, the co-simulation model is more reasonable than the traditional methods with simple virtual model. Based on these analyses, the sensibility of different vehicle parameters to its yaw stability is studied. Due to the ability of prediction and boundary treatment of MPC, it is used for the differential drive control development with the decoupling analyses of vehicle dynamic model. In order to produce the oscillatory yaw motion in prediction model of MPC for its control, the EKF is implemented to observe the real external disturbance with the guidance of nonlinear vehicle dynamic model. Case study under certain vehicle parameters and quantitative external disturbance is conducted to verify the analyses above. The results demonstrated that the designed controller can reduce the oscillation amplitude and period of vehicle yaw motion for about 40% and 80% respectively, which improve the vehicle stability greatly. Future work will focus on the practical application in the real DAHVs.

APPENDIX

(I-1)–(I-4), as shown at the bottom of the previous page, where $K11$-$K43$ can be expressed by

$$\begin{cases} K_{11} = \dfrac{A_1B_3C_2 - AB_2C_3}{m_1KK}, \quad K_{12} = \dfrac{A_1B_1C_3}{m_1KK}, \\ \quad K_{13} = \dfrac{-A_1B_1C_2}{m_1KK} \\ K_{21} = \dfrac{A_1A_2C_3 - A_1A_3C_2}{m_1KK}, \quad K_{22} = -\dfrac{A_1^2C_3}{m_1KK}, \\ \quad K_{23} = \dfrac{A_1^2C_2}{m_1KK} \\ K_{31} = Z\dfrac{A_1A_2C_3 - A_1A_3C_2}{KK}, \quad K_{32} = -Z\dfrac{A_1^2C_3}{KK}, \\ \quad K_{33} = Z\dfrac{A_1^2C_2}{KK} \\ K_{41} = \dfrac{-\left(A_1B_3 - A_3B_1\right)A_2 + \left(A_1B_2 - A_2B_1\right)A_3}{KK}, \\ \quad K_{42} = \dfrac{\left(A_1B_3 - A_3B_1\right)A_1}{KK}, \\ K_{43} = \dfrac{-\left(A_1B_2 - A_2B_1\right)A_1}{KK} \end{cases} \tag{I-5}$$

$$D = \begin{bmatrix} \dfrac{m_2\cos(\theta)}{m_1} & \dfrac{m_2\sin(\theta)}{m_1} & \dfrac{m_2L_f\sin(\theta)}{I_{zf}} & -1 & 0 & 0 \\ -\dfrac{m_2\sin(\theta)}{m_1} & \dfrac{m_2\cos(\theta)}{m_1} & \dfrac{m_2L_f\cos(\theta)}{I_{zf}} & 0 & -1 & 0 \\ 0 & 0 & 0 & 0 & 0 & -1 \end{bmatrix} \tag{I-8}$$

$$K' = \begin{bmatrix} \dfrac{1}{m_1} & 0 & 0 & 0 & 0 & 0 \\ 0 & \dfrac{1}{m_1} & 0 & 0 & 0 & 0 \\ 0 & 0 & \dfrac{1}{I_{zf}} & 0 & 0 & 0 \\ 0 & 0 & 0 & 0 & 0 & 0 \end{bmatrix} \tag{I-9}$$

$$A_{mpc} = \left(KD + K'\right)\begin{bmatrix} 0 & -m_1\omega_{f0} & -m_1v_{yf0} & 0 \\ m_1\omega_{f0} & 0 & m_1v_{xf0} & 0 \\ 0 & 0 & 0 & 0 \\ m_2\omega_{f0}\sin(\theta) & -m_2\omega_{f0}\cos(\theta) & m_2v_{xf0}\sin(\theta) - m_2v_{yf0}\cos(\theta) \\ & & -2m_2\cos(\theta)L_f\omega_{f0} & -2m_2\omega_{r0}L_r \\ m_2\omega_{f0}\cos(\theta) & m_2\omega_{f0}\sin(\theta) & m_2v_{xf0}\cos(\theta) + m_2v_{yf0}\sin(\theta) & 0 \\ & & -2m_2\sin(\theta)L_f\omega_{f0} & \\ 0 & 0 & 0 & 0 \end{bmatrix} \tag{I-10}$$

$$B_{mpc} = \left(KD + K'\right)\begin{bmatrix} 0 & 0 \\ 0 & 0 \\ 1 & 0 \\ 0 & 0 \\ 0 & 0 \\ 0 & 1 \end{bmatrix} \tag{I-11}$$

where $A1\sim A3$, $B1\sim B3$, $C2\sim C3$, KK, and U are shown in (I-6).

$$\begin{cases} A_1 = \left(\dfrac{m_2}{m_1}+1\right)\cos(\theta), \\ \quad B_1 = \left(\dfrac{m_2}{m_1}+\dfrac{m_2 L_f}{I_{zf}}\left(a-L_{fO}\right)+1\right)\sin(\theta) \\ A_2 = \left(-1-\dfrac{m_2}{m_1}\right)\sin(\theta), \\ \quad B_2 = \left(\dfrac{m_2}{m_1}+\dfrac{m_2 L_f}{I_{zf}}\left(a-L_{fO}\right)+1\right)\cos(\theta), \\ \quad C_2 = -m_2 L_r \\ A_3 = (b-L_{rO})\sin(\theta), B_3 = -(b-L_{rO})\cos(\theta), \\ \quad C_3 = -I_{zr}, \\ Z = \dfrac{a-L_{fO}}{I_{zf}}, KK = -(A_1B_3 - A_3B_1)AC_2 \\ \quad +(A_1B_2 - A_2B_1)A_1C_3 \end{cases} \tag{I-6}$$

$$\varphi_{ekf} = \left[\begin{array}{cc|c} \multicolumn{2}{c|}{A_{mpc}} & B_{mpc} \\ \hline 0 & 0 & 0 \\ 0 & 0 & 0 \end{array}\right] \tag{I-7}$$

where A_{mpc} and B_{mpc} are shown in (I-10) and (I-11), respectively.

REFERENCES

[1] Q. Gu, L. Liu, G. Bai, K. Li, Y. Meng, and F. Ma, "Longitudinal and lateral trajectory planning for the typical duty cycle of autonomous load haul dump," *IEEE Access*, vol. 7, pp. 126679–126695, 2019.

[2] T. Xu, Y. Shen, J. Xie, and W. Zhang, *Study of Hydraulic Steering Process for Intelligent Autonomous Articulated Vehicle*. Warrendale, PA, USA: SAE, 2018.

[3] T. Xu, Y. Shen, Y. Huang, and A. Khajepour, "Study of hydraulic steering process for articulated heavy vehicles based on the principle of the least resistance," *IEEE/ASME Trans. Mechatronics*, vol. 24, no. 4, pp. 1662–1673, Aug. 2019.

[4] P. A. Dudziski, "Design characteristics of steering systems for mobile wheeled Earthmoving equipment," *J. Terramechan.*, vol. 26, no. 1, pp. 25–82, Jan. 1989.

[5] D. N. L. Horton and D. A. Crolla, "Theoretical analysis of the steering behaviour of articulated frame steer vehicles," *Vehicle Syst. Dyn.*, vol. 15, no. 4, pp. 211–234, Jan. 1986.

[6] Y. Gao, Y. Shen, T. Xu, W. Zhang, and L. Guvenc, "Oscillatory yaw motion control for hydraulic power steering articulated vehicles considering the influence of varying bulk modulus," *IEEE Trans. Control Syst. Technol.*, vol. 27, no. 3, pp. 1284–1292, May 2019.

[7] N. L. Azad, A. Khajepour, and J. McPhee, "Analysis of jackknifing in articulated steer vehicles," in *Proc. IEEE Vehicle Power Propuls. Conf.*, Oct. 2005, pp. 86–90.

[8] Y. He, A. Khajepour, J. McPhee, and X. Wang, "Dynamic modelling and stability analysis of articulated frame steer vehicles," *Int. J. Heavy Veh. Syst.*, vol. 12, no. 1, pp. 28–59, 2004.

[9] Y. Gao, Y. Shen, Y. Yang, W. Zhang, and L. Guvenc, "Modelling, verification and analysis of articulated steer vehicles and a new way to eliminate jack-knife and snaking behavior," *Int. J. Heavy Veh. syst.*, vol. 26, nos. 3–4, pp. 375–404, 2019.

[10] N. L. Azad, A. Khajepour, and J. McPhee, "Effects of locking differentials on the snaking behaviour of articulated steer vehicles," *Int. J. Veh. Syst. Model. Test.*, vol. 2, no. 2, pp. 101–127, 2007.

[11] N. L. Azad, A. Khajepour, and J. McPhee, *Stability Control of Articulated Steer Vehicles by Passive and Active Steering Systems*. Warrendale, PA, USA: SAE, 2005.

[12] N. Lashgarian Azad, A. Khajepour, and J. Mcphee, "Robust state feedback stabilization of articulated steer vehicles," *Vehicle Syst. Dyn.*, vol. 45, no. 3, pp. 249–275, Mar. 2007.

[13] N. L. Azad, A. Khajepour, and J. McPhee, "Robust stabilization of articulated steer vehicles by differential braking," in *Proc. CSME Forum, Symp. Intell. Vehicles Transp. Syst.*, Calgary, BC, Canada, 2006, pp. 1–5.

[14] H. Cherouat and S. Diop, "An observer and an integrated braking/traction and steering control for a cornering vehicle," in *Proc. Amer. Control Conf.*, 2005, pp. 2212–2217.

[15] H. Peng and D. Eisele, "Vehicle dynamics control with rollover prevention for articulated heavy trucks," in *Proc. 5th Int. Symp. Adv. Vehicle Control*, Ann Arbor, MN, USA, 2000, pp. 1–8.

[16] J. J. Chun, P. Wang, Y. Shen, and J. Michael, "Differential control strategy based on an equal slip rate for an all-wheel electric-drive underground articulated dumping truck," *J. Eng. Sci. Tech. Rev.*, vol. 7, no. 4, pp. 163–168, 2014.

[17] T. Xu, X. Ji, and Y. Shen, "A novel assist-steering method with direct yaw moment for distributed-drive articulated heavy vehicle," *P. I. Mech. Eng. K, J. Mul.*, vol. 234, no. 1, pp. 214–224, 2020.

[18] Y. Yin, S. Rakheja, and P.-E. Boileau, "Multi-performance analyses and design optimisation of hydro-pneumatic suspension system for an articulated frame-steered vehicle," *Vehicle Syst. Dyn.*, vol. 57, no. 1, pp. 108–133, Jan. 2019.

[19] J. Tang, Y. Gao, H. Yu, Y. Wang, Y. Ai, and D. Cao, "Real-time display method for mining vehicle simulation based on virtual reality," in *Proc. IEEE 28th Int. Symp. Ind. Electron. (ISIE)*, Jun. 2019, pp. 1530–1535.

[20] D. A. Crolla, "The steering behaviour of articulated body steer vehicles," in *Proc. Int. Mech. Eng. Conf.*, 1983, pp. 1–10.

[21] E. Regolin, A. Alatorre, M. Zambelli, and A. C. Victorino, "A sliding-mode virtual sensor for wheel forces estimation with accuracy enhancement via EKF," *IEEE Trans. Veh. Tech.*, vol. 68, no. 4, pp. 3457–3471, Oct. 2019.

[22] A. Giannitrapani, N. Ceccarelli, F. Scortecci, and A. Garulli, "Comparison of EKF and UKF for spacecraft localization via angle measurements," *IEEE Trans. Aerosp. Electron. Syst.*, vol. 47, no. 1, pp. 75–84, May 2011.

[23] Y. Liu, X. Ji, K. Yang, X. He, X. Na, and Y. Liu, "Finite-time optimized robust control with adaptive state estimation algorithm for autonomous heavy vehicle," *Mech. Syst. Signal Process.*, vol. 139, May 2020, Art. no. 106616.

[24] C. Hu, R. Wang, F. Yan, Y. Huang, H. Wang, and C. Wei, "Differential steering based yaw stabilization using ISMC for independently actuated electric vehicles," *IEEE Trans. Intell. Transp. Syst.*, vol. 19, no. 2, pp. 627–638, Feb. 2018.

TAO XU (Member, IEEE) received the B.S. degree in vehicle engineering from the Shandong University of Science and Technology, China, in 2013, and the Ph.D. degree in mechanical engineering from the University of Science and Technology, Beijing, China, in 2019. He holds a postdoctoral position at the State Key Laboratory of Automotive Safety and Energy, Tsinghua University, Beijing. He is working on articulated heavy vehicle design and control; vehicle dynamics and control.

XUEWU JI received the B.S., M.S., and Ph.D. degrees in automotive engineering from the College of Automotive Engineering, Jilin University, Changchun, China, in 1987, 1990, and 1994, respectively. He is currently an Associate Professor with the State Key Laboratory of Automotive Safety and Energy, Tsinghua University, Beijing, China. His research interests include vehicle dynamics and control, and advanced steering system technology. He was a recipient of the National Science and Technology Progress Award for his achievements in the industrialization of electric power steering technology, in 2014.

YULONG LIU received the B.S. degree from the Hefei University of Technology, China, in 2016. He is currently pursuing the Ph.D. degree in mechanical engineering with the State Key Laboratory of Automotive Safety and Energy, Tsinghua University, China. His research interests include vehicle dynamics and control, driver-vehicle shared control, and motion planning for automated vehicle.

YAHUI LIU (Member, IEEE) received the B.S. degree from Jilin University, Changchun, China, in 2003, and the Ph.D. degree from Beihang University, Beijing, China, in 2009, all in automotive engineering. He is currently an Associate Professor with the State Key Laboratory of Automotive Safety and Energy, Tsinghua University, Beijing. His research interests include driver-vehicle system dynamics, driver-vehicle automation collaboration, and shared control.